Journal of Oceanology and Limnology
Vol. 35 No. 1, P. 23-38, 2017
http://dx.doi.org/10.1007/s00343-016-5178-y

Climate variability and predictability associated with the Indo-Pacific Oceanic Channel Dynamics in the CCSM4 Coupled System Model*

YUAN Dongliang (袁东亮)[1, 2, **], XU Peng (徐鹏)[1, 3], XU Tengfei (徐腾飞)[4]

[1] *Key Laboratory of Ocean Circulation and Waves* (*KLOCAW*), *Institute of Oceanology*, *Chinese Academy of Sciences*, *Qingdao 266071*, *China*

[2] *Qingdao Collaborative Innovation Center of Marine Science and Technology*, *Qingdao 266003*, *China*

[3] *University of Chinese Academy of Sciences*, *Beijing 100049*, *China*

[4] *First Institute of Oceanography*, *State Oceanic Administration*, *Qingdao 266061*, *China*

Received Jun. 12, 2015; accepted in principle Aug. 15, 2015; accepted for publication Oct. 19, 2015

Abstract An experiment using the Community Climate System Model (CCSM4), a participant of the Coupled Model Intercomparison Project phase-5 (CMIP5), is analyzed to assess the skills of this model in simulating and predicting the climate variabilities associated with the oceanic channel dynamics across the Indo-Pacific Oceans. The results of these analyses suggest that the model is able to reproduce the observed lag correlation between the oceanic anomalies in the southeastern tropical Indian Ocean and those in the cold tongue in the eastern equatorial Pacific Ocean at a time lag of 1 year. This success may be largely attributed to the successful simulation of the interannual variations of the Indonesian Throughflow, which carries the anomalies of the Indian Ocean Dipole (IOD) into the western equatorial Pacific Ocean to produce subsurface temperature anomalies, which in turn propagate to the eastern equatorial Pacific to generate ENSO. This connection is termed the "oceanic channel dynamics" and is shown to be consistent with the observational analyses. However, the model simulates a weaker connection between the IOD and the interannual variability of the Indonesian Throughflow transport than found in the observations. In addition, the model overestimates the westerly wind anomalies in the western-central equatorial Pacific in the year following the IOD, which forces unrealistic upwelling Rossby waves in the western equatorial Pacific and downwelling Kelvin waves in the east. This assessment suggests that the CCSM4 coupled climate system has underestimated the oceanic channel dynamics and overestimated the atmospheric bridge processes.

Keyword: Indian Ocean Dipole; El Niño-Southern Oscillations (ENSO); oceanic channel; Community Climate System Model (CCSM4); Indonesian Throughflow; ENSO predictability

1 INTRODUCTION

The variability of the Pacific and Indian Oceans is of great importance to global climate variability and predictability. Within the Pacific and Indian Oceans, El Niño-Southern Oscillation (ENSO) and Indian Ocean Dipole (IOD) are strong interannual modes of climate variability. The tropical Indian Ocean warming, which is the primary mode of Indian Ocean sea surface temperature (SST) anomalies, has been shown to act like a capacitor anchoring the atmospheric anomalies resulting from ENSO (Ohba and Ueda, 2005; Ohba and Ueda, 2009b; Xie et al., 2009) and subsequently has an influence on ENSO through the Walker circulation (Klein et al., 1999; Annamalai et al., 2005; Kug and Kang, 2006; Ohba and Ueda, 2007; Ohba and Watanabe, 2012). Moreover, the IOD

* Supported by the National Basic Research Program of China (973 Program) (No. 2012CB956000), the Strategic Priority Project of Chinese Academy of Sciences (No. XDA11010301), the National Natural Science Foundation of China (Nos. 41421005, U1406401), the Public Welfare Grant of China Meteorological Administration (No. GYHY201306018), and the Global Change and Air-Sea Interactions of State Oceanic Administration (No. GASI-03-01-01-05)
** Corresponding author: dyuan@qdio.ac.cn

also interacts with ENSO through the Walker circulation (Klein et al., 1999; Alexander et al., 2002; Clarke and van Gorder, 2003; Lau and Nath, 2003; Lau et al., 2005; Kug et al., 2006; Luo et al., 2010; Izumo et al., 2010). In this study, the IOD forcing process on ENSO is called the atmospheric bridge. In addition to the atmospheric bridge, the role of the Indonesian Throughflow (ITF) in connecting the interannual variabilities of the Indian Ocean with those of the Pacific Ocean was recently uncovered by Yuan et al. (2011, 2013), showing that the upwelling anomalies in the southeastern tropical Indian Ocean during the IOD induce anomalous transport through the Indonesian seas. This anomalous transport elevates the thermocline of the western Pacific warm pool and produces subsurface temperature anomalies in the western equatorial Pacific, which propagate to the eastern Pacific cold tongue to induce significant climate variations at a time lag of 1 year. This process was named "oceanic channel dynamics" by Yuan et al. (2011), and behaves in opposition to the atmospheric bridge process. Analyses have suggested that the oceanic channel dynamics hold the key to the interannual predictability of the tropical Indo-Pacific climate variations across the spring barrier because of the persistency of the thermocline anomalies (Yuan et al., 2011). The oceanic channel dynamics are evidenced by the significant lag correlations between the oceanic anomalies in the southeastern tropical Indian Ocean in autumn and those in the cold tongue and in the Pacific equatorial vertical section in the 1-year time lag. This suggests that the oceanic thermocline processes are important in determining the variability and predictability of the Pacific climate (Yuan et al., 2013).

The lag correlation analyses conducted on observational data by Yuan et al. (2013) can be applied to numerical results produced by modern climate system models to assess the skills of the models in simulating and predicting the climatic variations associated with the oceanic channel dynamics. In this study, the skill of the Community Climate System Model version 4 (CCSM4) that participates in the Coupled Model Intercomparison Project phase-5 (CMIP5) is assessed using the same lag correlation analyses as Yuan et al. (2013) to evaluate the skill of the CCSM4 model in predicting ENSO and to identify model deficiencies. A similar analysis has been conducted by Xu et al. (2013) on the Flexible Global Ocean-Atmosphere-Land System Model (FGOALS) climate system model of China. The results of their study showed that the oceanic channel dynamics in FGOALS are overwhelmed by an artificially strong atmospheric bridge so that the predictability of ENSO using IOD as a precursor is greatly reduced in that model. In the current study, we conduct a similar analysis on the CCSM4 coupled model, which is a much more widely used climate system model in the international user community. In contrast to the FGOALS model simulation, the CCSM4 model simulates a realistic SST lag correlation between the southern tropical Indian Ocean and eastern Pacific, despite the weak ITF connectivity between IOD and ENSO from the 1-year lag. However, we will show that the model has actually simulated an unrealistic atmospheric bridge. The subsequent analysis will help us to understand the climate simulation with more insight into the dynamics of the system.

This paper is organized as follows. Section 2 introduces the data and the model experiment. Section 3 presents the results of the lag correlation analyses of the CCSM4 model simulation and compares them with analyses based on the observational data. Our conclusions are summarized in Section 4.

2 DATA AND MODEL

The observational data used in this study are the same as in Yuan et al. (2013). The Hadley Centre Sea Ice and Sea Surface Temperature dataset (HADISST; Rayner et al., 2003) covers the global ocean from 1870 to the near present with a resolution of 1°×1°. The sea surface height data are the merged altimeter data from Satellites Topex/Poseidon, Jason-1, and ERS, archived by the Aviso project on a 1/3° resolution grid globally since 1993 (ftp://ftp.aviso.oceanobs.com). The subsurface temperature data are obtained from the Joint Environmental Data Analysis Center (JEDAC) of the Scripps Institution of Oceanography, which are on a 5°×2° grid at 11 levels (0, 20, 40, 60, 80, 120, 160, 200, 240, 300, and 400 m) from 1990 to 2003 (White, 1995). The surface zonal wind data are the National Center for Environmental Prediction/National Center for Atmospheric Research (NCEP/NCAR) reanalysis data from a 2.5°×2.5° grid from 1987 to 2009 (Kalnay et al., 1996). The geostrophic transport of the ITF is calculated from the expendable bathythermograph (XBT) data across the IX1 section between Western Australia and Java Island. A statistical temperature-salinity relationship based on historical hydrographic data is used in the calculation (Meyers et al., 1995; Meyers, 1996; Wijffels and Meyers, 2004; Wijffels et al., 2008). The geostrophic

transport is calculated in reference to the 700-m level-of-no-motion. The time series covers the period from 1987 to 2008. Interannual monthly anomalies of the ITF geostrophic transport are calculated based on the monthly climatology from 1987 to 2008. The differences in the monthly climatology and interannual anomalies with or without the strong 1997–1998 El Niño are small, suggesting that the climatology and interannual anomalies are robust in our analyses.

We use the CCSM4 model in this study (Gent et al., 2011), which is a Coupled General Circulation Model (CGCM) composed of four geophysical model components: the Community Atmosphere Model (CAM4.0) (Neale et al., 2013), the Los Alamos Sea Ice Model (CICE4) (Hunke and Lipscomb, 2008), the Community Land Model version 4 (CLM4) (Lawrence et al., 2011), and the Parallel Ocean Program version 2 (POP2) (Smith et al., 2010). A coupler (CPL7) (Craig et al., 2012) is used to coordinate the communications among the four model components. The ocean component of CCSM4 employs a model grid of 1.125° resolution in the zonal direction and a varying meridional resolution increasing from 0.27° near the equator to 0.54° poleward of 33°N and 33°S. In the vertical direction, the ocean model contains 60 irregular levels with 16 layers in the upper 155 m. The atmospheric component of CCSM4 employs a 1.25°×0.9° grid at 26 layers in the vertical direction. The output from the land and ice component models is not used in this study. The detailed configurations of these models can be found in the CCSM4 user manual (http://www.cesm.ucar.edu/models/ccsm4.0/ccsm_doc/book1. html).

The "historical" simulations of CCSM4 based on the experimental design of CMIP5 (Taylor et al., 2012) are used in this study. CMIP5 has a standard experimental protocol for comparing the performance of CGCMs of the international communities (Meehl et al., 2000). The project promotes a set of model simulations to evaluate the skills of the models in simulating the recent past, based on which projections of future climate change (near or long term) are produced and factors responsible for the differences in model projections are output for analysis. We use one of the six ensemble member experiments (r1i1p1) of the CCSM4 historical simulation with both anthropogenic and natural forcing from the middle of the 19th century to 2005 to conduct the analyses in this study.

Several indices are used in this study. The Dipole Mode Index (DMI) is defined as the difference of area-averaged SST anomalies (SSTA) between the western (50°–70°E, 10°S–10°N) and southeastern (90°–110°E, 10°S–Equator) tropical Indian Ocean areas (Saji et al., 1999). The Niño3.4 index is calculated as the SSTA averaged in the area of the equatorial central-eastern Pacific (170°–120°W, 5°S–5°N). The surface zonal wind anomalies (SZWA) of the western equatorial Pacific are the averaged zonal wind anomalies over the area of 130°–150°E and 5°S–5°N.

Throughout this paper, the lag correlation is calculated as the correlation between the area-averaged oceanic anomalies in boreal autumn in the southeastern tropical Indian Ocean (90°–110°E, 10°S–Equator) or SZWA over the far western equatorial Pacific Ocean and the anomalies over the Indo-Pacific Oceans in other seasons (the following winter until autumn). Boreal seasons are used throughout this paper. They are defined as spring (March to May), summer (June to August), autumn (September to November), and winter (December to the following February). Throughout this paper, the IOD year is represented by Year 1 and the following year is represented by Year 2.

3 RESULT

3.1 Model validation

The ENSO and IOD events in the historical simulations of CGCM generally do not correspond well with the real events because of the initialization of the historical simulations from an arbitrary point of a quasi-equilibrium control run. The internal interactions within the nonlinear climate system are usually not as predictable as the variabilities produced by the external natural and anthropologic forcing (Taylor et al., 2012). However, the averaged periodicity and amplitudes of the simulated interannual events can be compared with those in nature. We selected one of the six ensemble member experiments (r1i1p1) in which the best simulation of the ENSO events in nature was achieved. We then shifted the time coordinates of the simulated interannual events to match a strong ENSO event with the observations from the 1997–1998 ENSO so that the recurrences of ENSO and IOD during a few decades can be compared with the observations. This is essentially equivalent to a coupled initialization for a better hindcast and prediction.

The simulated Niño3.4 index and DMI after the shift was applied was then compared with the indices

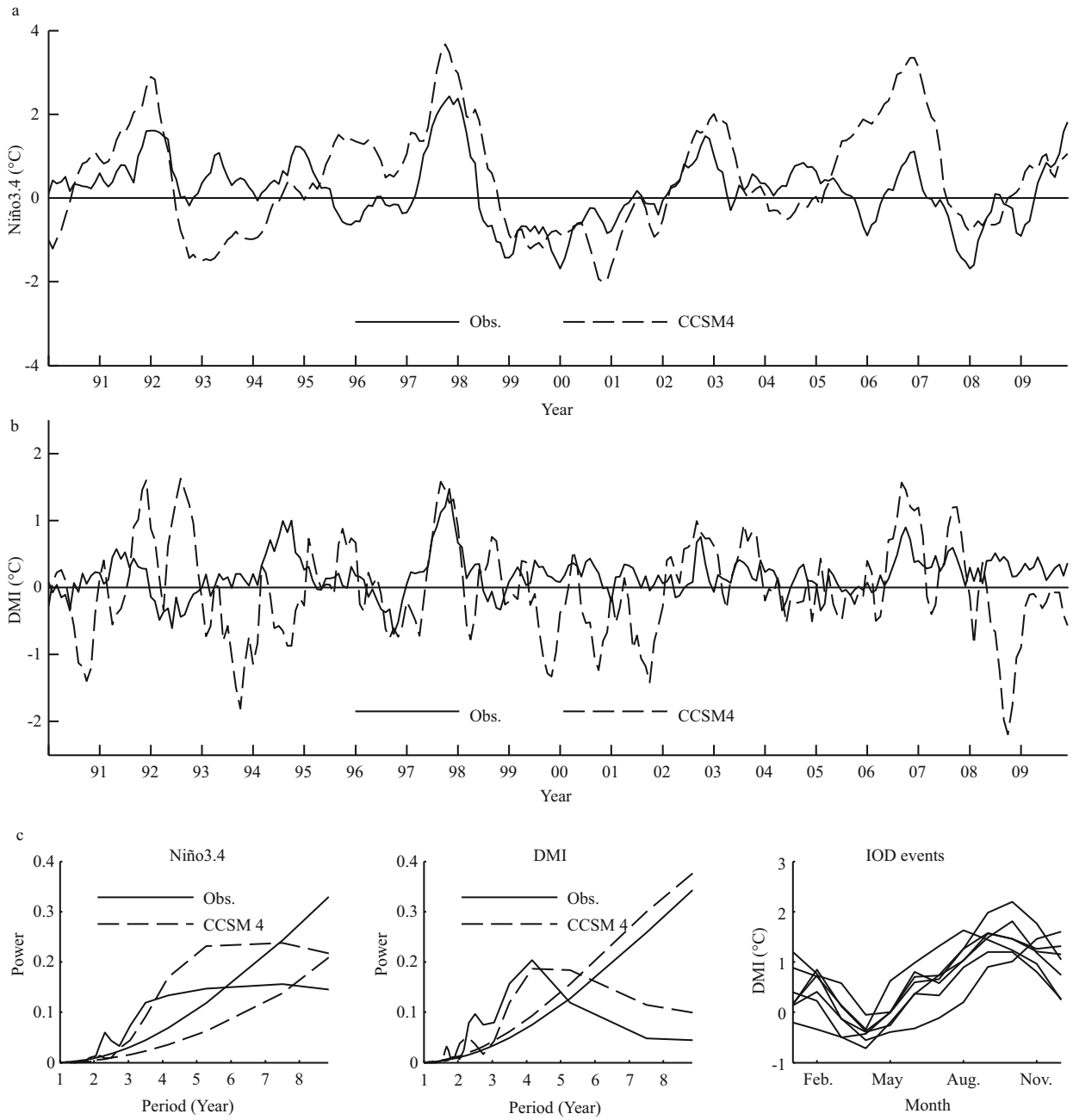

Fig.1 Comparison of Niño3.4 index (a) and DMI (b) of the HADISST (solid line) and the CCSM4 simulation (dashed line); the bottom panel (c) shows the power spectra of the Niño3.4 index and DMI, and the dispersion of DMI of the simulated IOD events by CCSM4

The smooth curves in the spectra plots indicate the 95% confidence level. The correlation coefficient between the observed and simulated Niño3.4 index is 0.51, above the 95% confidence level.

calculated from the HADISST data during 1990 to 2009. This analysis shows that the model has reproduced well the ENSO and IOD events since 1990 (Fig.1). The spectral analyses confirm that the CCSM4 simulation has successfully reproduced the periodicity and amplitudes of the observed ENSO and IOD events in the past two decades. Analyses also suggest that the phase-locking of the IOD with the autumn season has been reproduced successfully in the CCSM4 simulation (Fig.1c).

The skill of the CCSM4 model system in simulating the ENSO and IOD events is further indicated by the regression coefficients between the DMI index with the SSTA in the Indian Ocean and by the regression coefficients between the Niño3.4 index with the SSTA in the Pacific Ocean. The similar spatial patterns

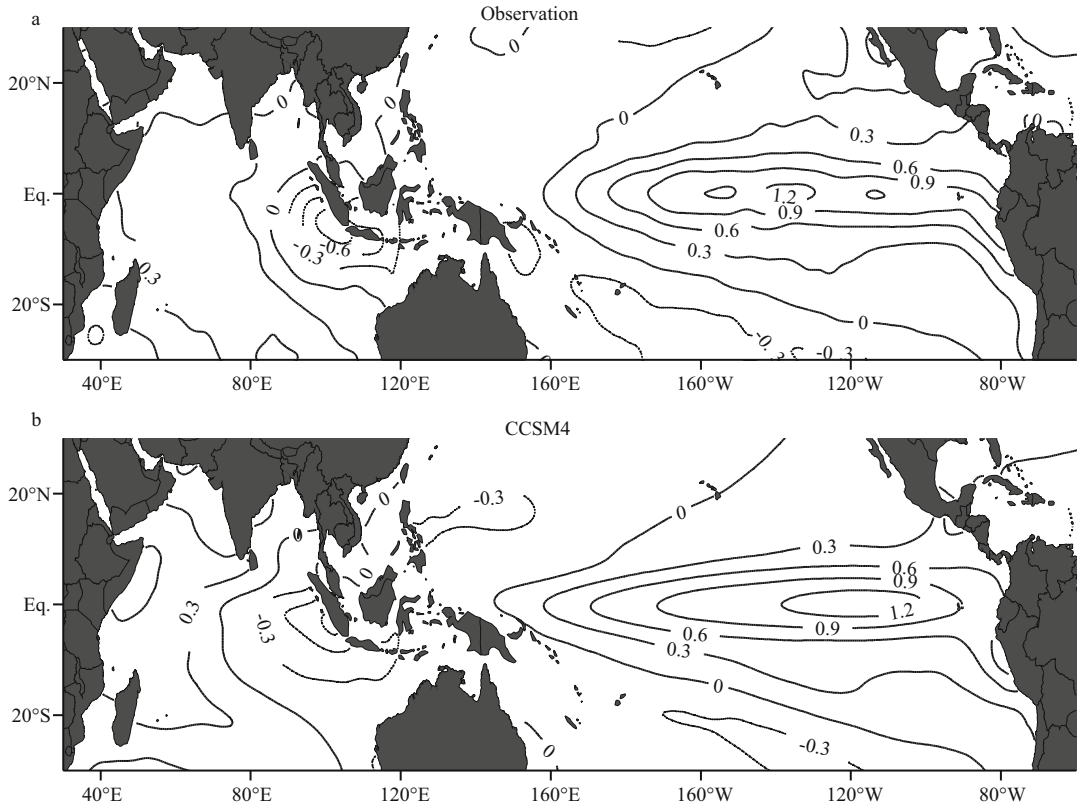

Fig.2 Comparison of the observed (a) and simulated (b) regression coefficients between the DMI index and the SSTA in the Indian Ocean and between the Niño3.4 index and the SSTA in the Pacific Ocean

The simulated regression coefficients are calculated based on the simulated DMI and Niño3.4 index.

between the regression coefficients in the simulation and those in the observations suggest that the CCSM4 coupling system is capable of simulating well the observed IOD and ENSO spatial patterns over the Indo-Pacific basins (Fig.2).

3.2 Lag correlation of SSTA

The southeastern tropical Indian Ocean is the eastern pole of the IOD events, which usually peak in autumn, so the area-averaged SSTA in this region in autumn are used to represent IOD signals. Figure 3 shows the lag correlations between the SSTA in the southeastern tropical Indian Ocean in autumn and the Indo-Pacific SSTA from the following winter until autumn. The significant lag correlations above the 95% confidence level show the IOD-ENSO type teleconnections clearly in winter both in the observations and in the model, with positive correlations in the western Pacific and eastern Indian Oceans, and negative correlations in the eastern Pacific and western Indian Oceans (Fig.3a). The lag correlations subside in spring in both the observations and the model, consistent with the existence of the spring barrier. The significant lag correlations re-emerge in the cold tongue in the summer through autumn of Year 2, exceeding the 95% confidence level in both the observations and the model, but with the opposite sign to those in winter. The significant lag correlations in the 1-year time lag suggest that some ENSO events can be predicted effectively beyond the spring barrier if the IOD should be used as a precursor.

It is clear that the lag correlations in the cold tongue in the autumn of Year 2 are stronger and take place over a larger longitudinal domain in the model than in the observations. The difference is attributed to unrealistic westerly wind anomalies in the western-central equatorial Pacific in the model during the decay phase of the ENSO-IOD events, which will be discussed in detail later in Section 3.6.

The lag correlations between the SSTA in the southeastern Indian Ocean in autumn and in the cold tongue with the ENSO signals removed in the 1-year time lag remain significant above the 95% confidence level in both the observational and model results (figure omitted), suggesting that the predictability is independent of ENSO. The dynamics of the significant lag correlations independent of the tropical Pacific

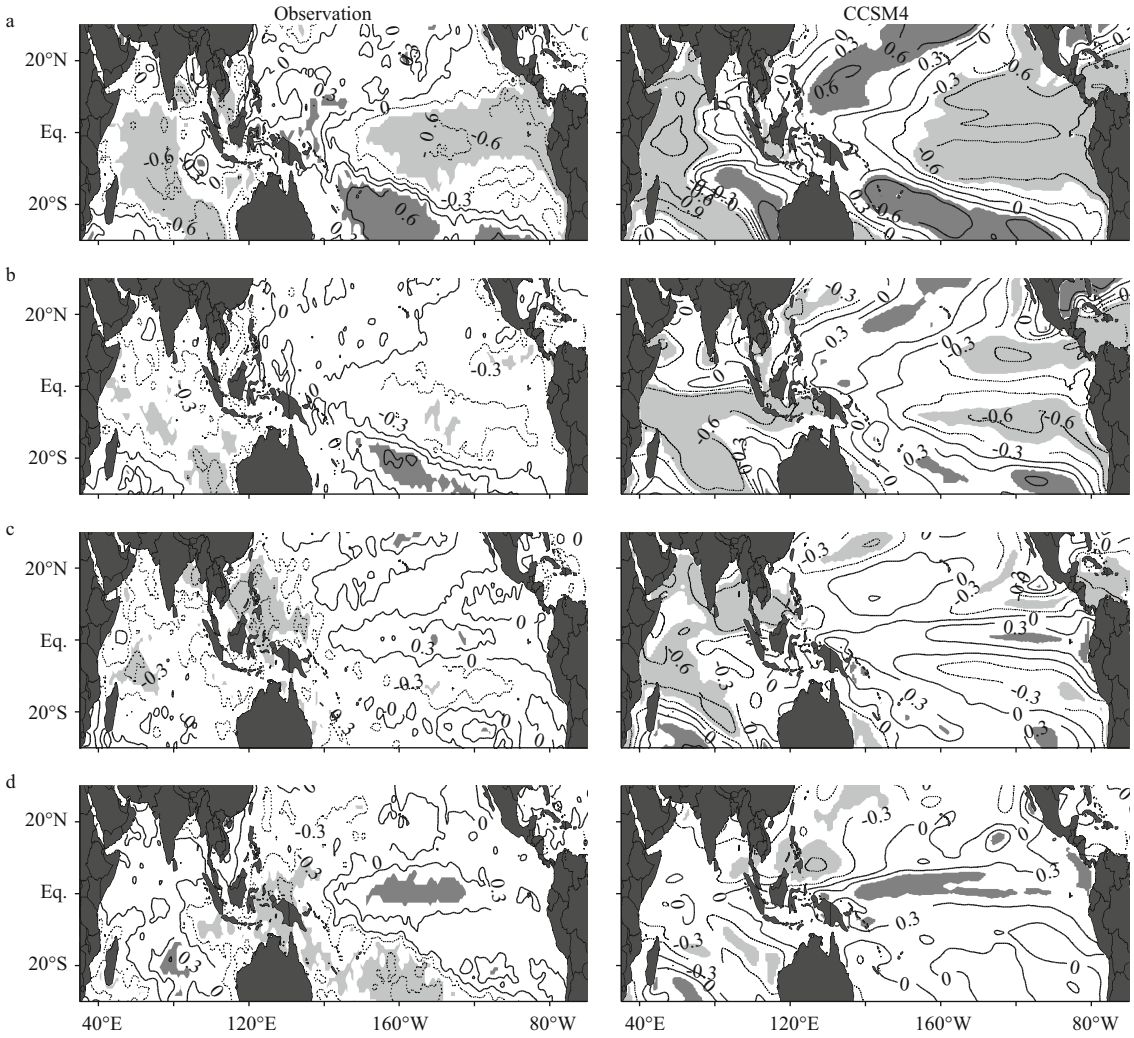

Fig.3 Comparison of observed (left column) and simulated (right column) lag correlations between the SSTA in the southeastern tropical Indian Ocean in autumn and the tropical Indo-Pacific SSTA in the following four seasons for the period of 1990 to 2009

a. winter (December to February); b. spring (March to May); c. summer (June to August); d. autumn (September to November). The contour interval is 0.3. Dark and light shades indicate positive and negative correlations significant at the 95% confidence level, respectively.

air-sea coupling have been explained by Yuan et al. (2011, 2013) showing that the equatorial Kelvin waves of the eastern Indian Ocean propagate into the Indonesian seas and change the ITF transport. The anomalous ITF transport then elevates the thermocline of the western Pacific warm pool and produces subsurface temperature anomalies in the western equatorial Pacific, which propagate further to the east to affect the cold tongue SSTA in the summer-autumn of Year 2. This thermocline process of IOD-forced equatorial Pacific climate variations through the ITF variability is termed the "oceanic channel dynamics" (Yuan et al., 2011, 2013).

In the CCSM4 simulation, the lag correlations between the warm pool SSTA in autumn and the cold tongue SSTA in the spring until the autumn of Year 2 are insignificant [figure omitted, the warm pool is defined as the area endorsed by the 28.5°C contour], which indicates that the SSTA in the cold tongue in the autumn of Year 2 did not originate from the warm pool. This result is consistent with the observational analysis by Yuan et al. (2013).

3.3 Lag correlation of SSHA

Figure 4 shows that the lag correlations between the SSHA in the southeastern tropical Indian Ocean in autumn and the Indo-Pacific SSHA in the following winter until autumn in the CCSM4 simulation on the equator are in good agreement with those based on the satellite altimeter sea-level data. Similar to the SSTA lag correlations, a typical IOD-ENSO teleconnection is indicated by the SSHA lag

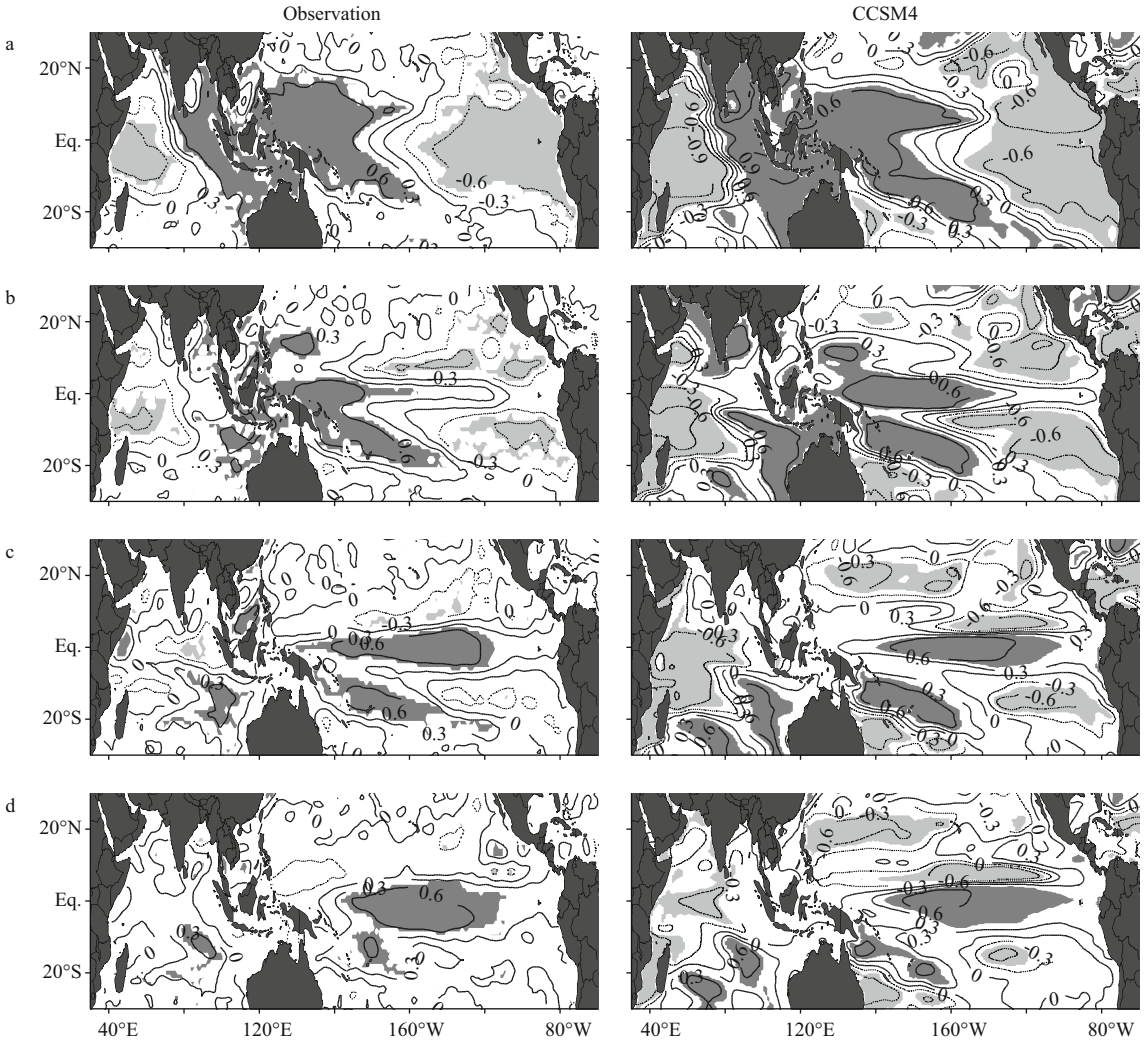

Fig.4 Comparison of observed (left column) and simulated (right column) lag correlations between the SSHA in the southeastern tropical Indian Ocean in autumn and the tropical Indo-Pacific SSHA in the following four seasons for the period of 1993 to 2009

a. winter (December to February); b. spring (March to May); c. summer (June to August); d. autumn (September to November). The contour interval is 0.3. Dark and light shades indicate positive and negative correlations significant at the 95% confidence level, respectively.

correlations in the immediate winter following the IOD, with the lag correlations in the eastern Indian Ocean and western Pacific showing the opposite sign to those in the western Indian Ocean and eastern Pacific cold tongue (Fig.4a). The lag correlations in spring suggest that the interannual anomalies from the eastern Indian Ocean have propagated into the Indonesian seas to induce the anomalous ITF transport, which elevates the thermocline and produces subsurface temperature anomalies in the western equatorial Pacific Ocean in both the model and the observations (Fig.4b). The anomalies reach the central and eastern equatorial Pacific Ocean in the summer and autumn seasons of Year 2, as indicated by the movement of the significant positive correlations in Fig.4c and d. The eastward propagation of the significant correlations is confined to a narrow equatorial band of the Pacific Ocean, suggesting the influence of the equatorial Kelvin waves. These comparisons suggest that the essential structure of the oceanic channel dynamics is simulated well by the CCSM4 simulation.

Similar to the SSTA lag correlations, the SSHA lag correlations in the cold tongue in autumn are stronger and over a larger longitudinal domain in the model than in the observations. The reasons for this difference will be explained in Section 3.6.

The lag correlations in the equatorial band of the Pacific Ocean remain significant even when the ENSO contributions associated with Niño3.4 index are removed from the Indo-Pacific SSHA time series (figure omitted). The results together with the SSTA

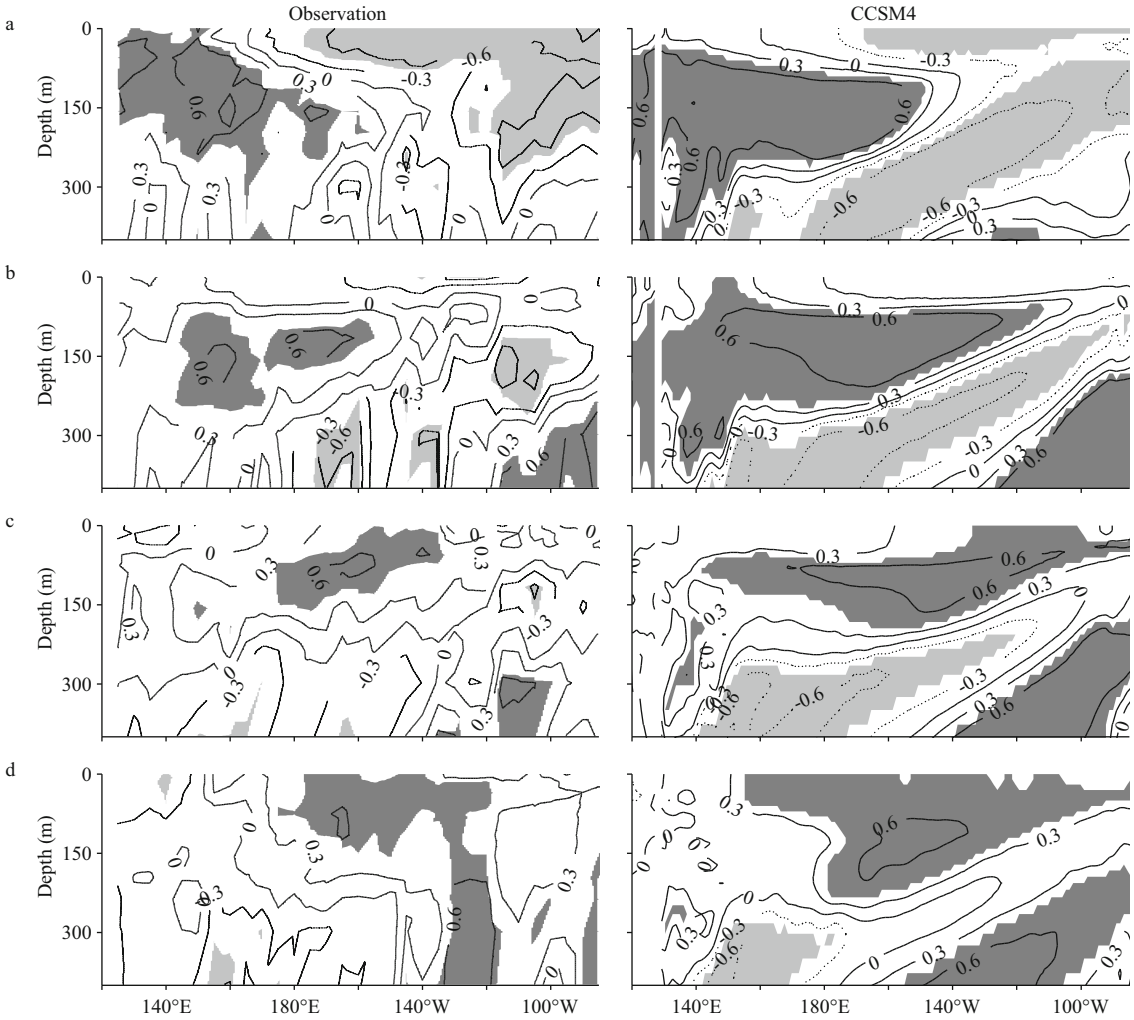

Fig.5 Comparison of observed (left column) and simulated (right column) lag correlations between the SSTA in the southeastern tropical Indian Ocean in autumn and the temperature anomalies in the Pacific equatorial vertical section in the following four seasons for the period of 1990 to 2003

a. winter (December to February); b. spring (March to May); c. summer (June to August); d. autumn (September to November). The contour interval is 0.3. Dark and light shades indicate positive and negative correlations significant at the 90% confidence level, respectively.

lag correlations indicate that the oceanic channel dynamics are independent of the tropical Pacific air-sea coupling. This characteristic has been simulated well by CCSM4, as evidenced by the good agreement of the non-ENSO SSHA and SSTA lag correlations with the observations.

3.4 Subsurface lag correlation

The oceanic channel dynamics are also suggested by the lag correlations in the subsurface equatorial Pacific Ocean. The lag correlations between the SSTA in the southeastern tropical Indian Ocean in autumn and the subsurface temperature anomalies in the equatorial Pacific vertical section in the following winter until autumn are shown in Fig.5. The significant lag correlations in winter show a dipole pattern with positive values in the western basin and negative in the eastern basin (Fig.5a), which are in agreement with the SSTA and SSHA lag correlations in Figs.3a and 4a. In spring, the surface lag correlations become insignificant, but the subsurface lag correlations remain significant and propagate to the east, then surface in the eastern Pacific cold tongue in the summer until the autumn of Year 2 (Fig.5b, c, d), producing the significant SSTA and SSHA lag correlations in the 1-year time lag shown in Figs.3d and 4d. The CCSM4 simulation reproduces well these subsurface lag correlations and their eastward propagation in the observations, except that the simulated subsurface lag correlations are much stronger than those in the observations. The potential predictability of ENSO beyond the spring barrier is

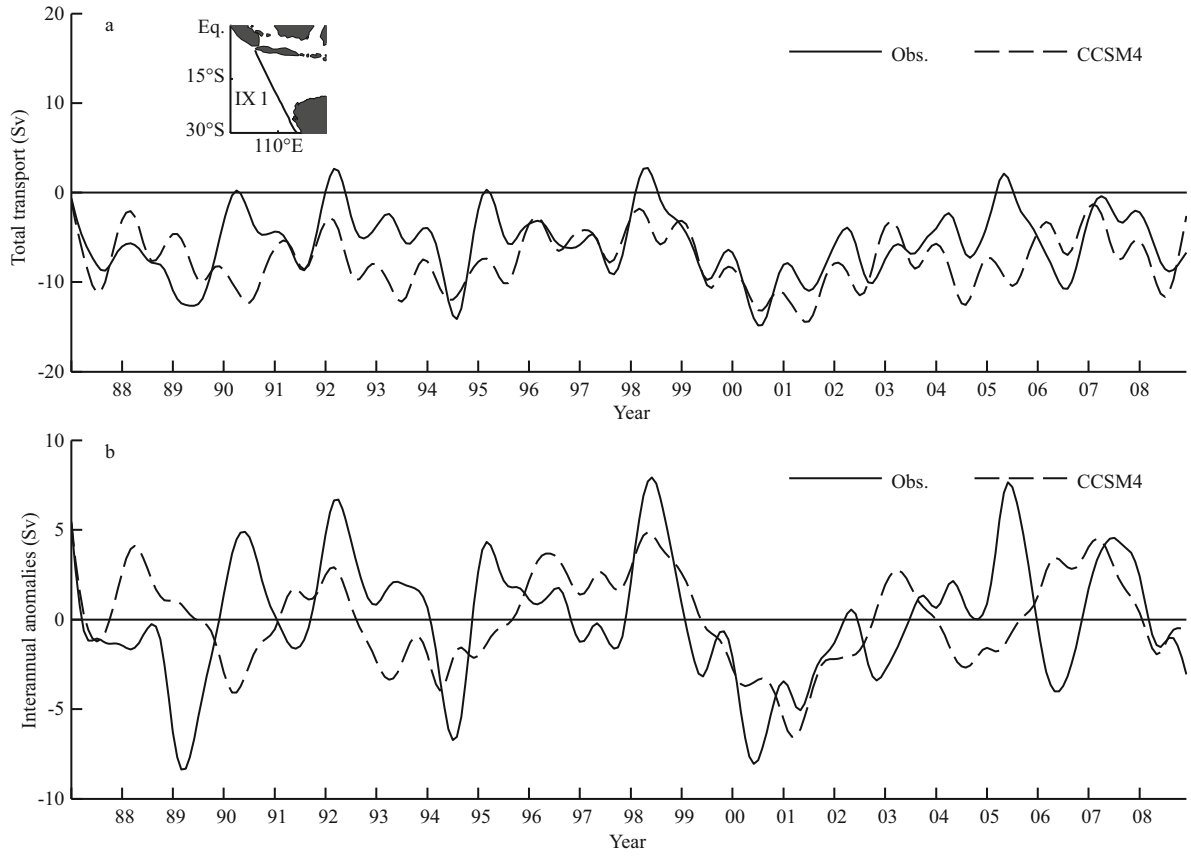

Fig.6 Comparison of observed and simulated geostrophic transport of ITF (a) and its interannual anomalies (b) across the IX1 section between Western Australia and Java over the period of 1987 to 2008

Solid and dashed lines represent the observed and simulated geostrophic transport reference to the 700-m level-of-no-motion across the IX1 section, respectively. The time series are low-pass filtered with a Butterworth window with a cutoff period at 13 months.

likely to be associated with the subsurface connections across the equatorial Pacific basin. The substantially stronger subsurface link in the CCSM4 simulation than in the observations explains the simulated stronger correlations between SSTA (SSHA) in the southeastern tropical Indian Ocean in autumn and the SSTA (SSHA) in the eastern Pacific cold tongue in the 1-year time lag (Figs.3d and 4d).

3.5 Variability of the ITF

The geostrophic transport of the ITF and its interannual anomalies across the IX1 section between Java and Western Australia are calculated from the CCSM4 simulation and compared with those based on the geostrophic transport of the XBT data (Fig.6). The CCSM experiment has simulated a mean geostrophic ITF transport of -7.6 Sv in comparison with the observed mean geostrophic transport of -5.7 Sv across the IX1 section, the agreement of which is above the 99% confidence level. The interannual anomalies of the simulated ITF geostrophic transport have a standard deviation of 3.97 Sv, which is smaller than that of the observed value (6.86 Sv). The correlation coefficient between the simulated and observed interannual anomalies of the ITF geostrophic transport is 0.31, above the 99% confidence level.

The sea levels in the northwestern Australian coast are known to be highly correlated with the equatorial Pacific zonal winds (the ENSO signal), whereas the sea levels in the southern Java coast are closely related to the interannual zonal winds over the equatorial Indian Ocean (the IOD signal) (Clarke and Liu, 1994; Meyers, 1996). We have divided the geostrophic transport across the IX1 section into two parts: the southern transport from the northwestern Australian coast to 15°S and the northern transport from the southern Java coast to 15°S, and present comparisons of the simulated and observed time series in these regions in Fig.7. The simulated and observed interannual anomalies of the southern transport have standard deviations of 1.88 Sv and 2.18 Sv, respectively. In comparison, the simulated and observed interannual anomalies of the northern transport have standard deviations of 3.41 Sv and

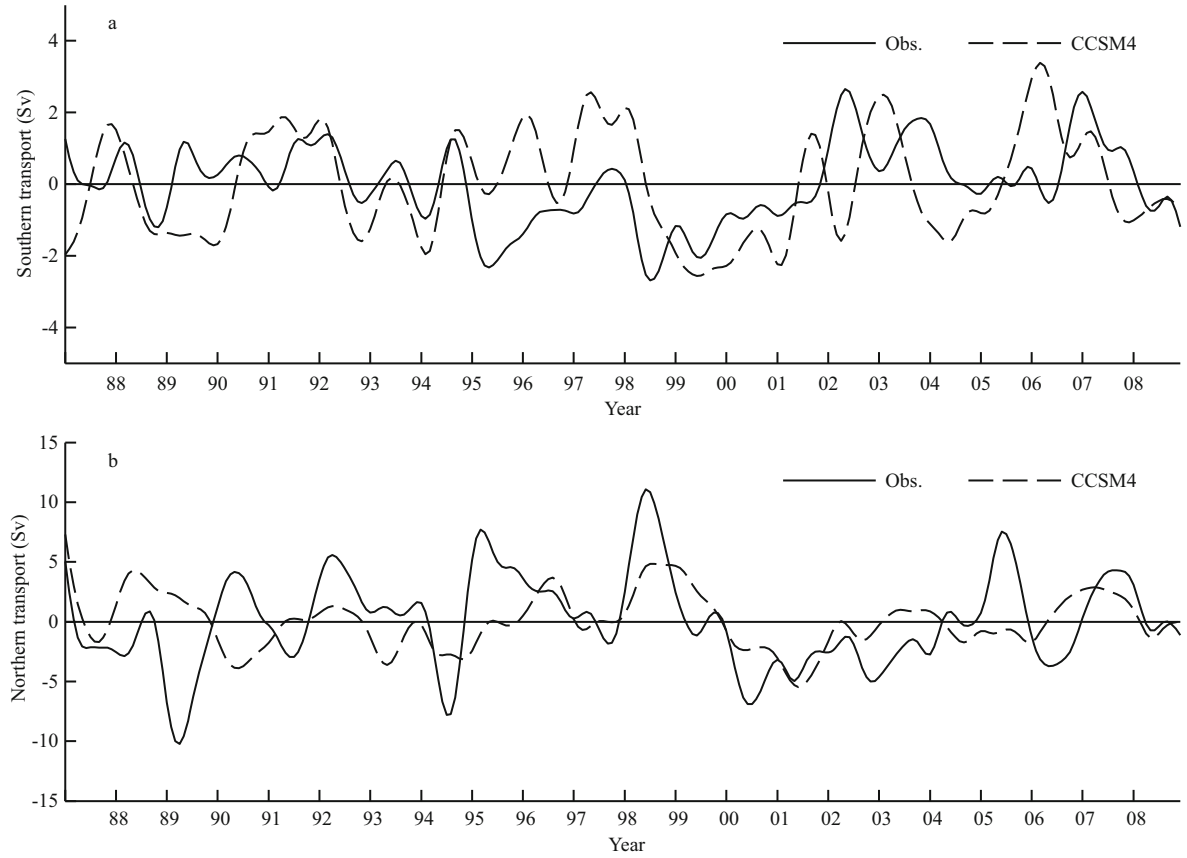

Fig.7 Comparison of observed and simulated interannual anomalies of the southern geostrophic transport from the northern Australian coast to 15°S (a) and the northern geostrophic transport from the southern Java coast to 15°S (b) across the IX1 section over the period of 1987 to 2008

Solid and dashed lines represent the observed and simulated geostrophic transport anomalies, respectively. The time series are low-pass filtered with a Butterworth window with a cutoff period at 13 months.

9.95 Sv, respectively. Evidently, the model simulates weaker northern interannual anomalies than observed, which indicates deficiencies of the model in simulating the ITF transport across the northern IX1 section (Fig.1).

In theory, the interannual anomalies of the southern and northern transport should be highly correlated with the ENSO and IOD indices, respectively. The lead-lag correlations between the southern interannual anomalies and the Niño3.4 or DMI index show that the correlations with the Niño3.4 index are significantly positive above the 99% level at the time lag between -8 to 4 months with a peak at a near-zero time lag (Fig.8c). This is consistent with the observations (Fig.8a) and the theory of Clarke and Liu (1994) and Meyers (1996). The correlations between the southern interannual anomalies and the DMI index are significantly positive at the near-zero time lag in the observations (Fig.8b), but are clearly overestimated by the CCSM4 simulation (Fig.8d). The artificial correlations between the southern anomalies and the DMI index at -12 to -6 months of time lag suggest model deficiencies in simulating the ITF transport across the southern IX1 section.

The model has successfully simulated the correlations between the interannual anomalies of the northern transport and the Niño3.4 index (Fig.9a, c). In contrast, the correlations of the northern anomalies with the DMI index are not simulated as successfully (Fig.9b, d). The difference suggests that the model is unable to successfully simulate the connection between IOD and the ITF interannual variability, the detailed investigation of which is beyond the scope of this study.

The underestimated oceanic channel dynamics in the simulation contrast with the stronger lag correlations in the subsurface equatorial vertical section of the Pacific Ocean in the model compared with in the observations. The stronger subsurface lag correlations are also supported by the stronger lag correlations in the model between the SSTA and SSHA in the southeastern tropical Indian Ocean in

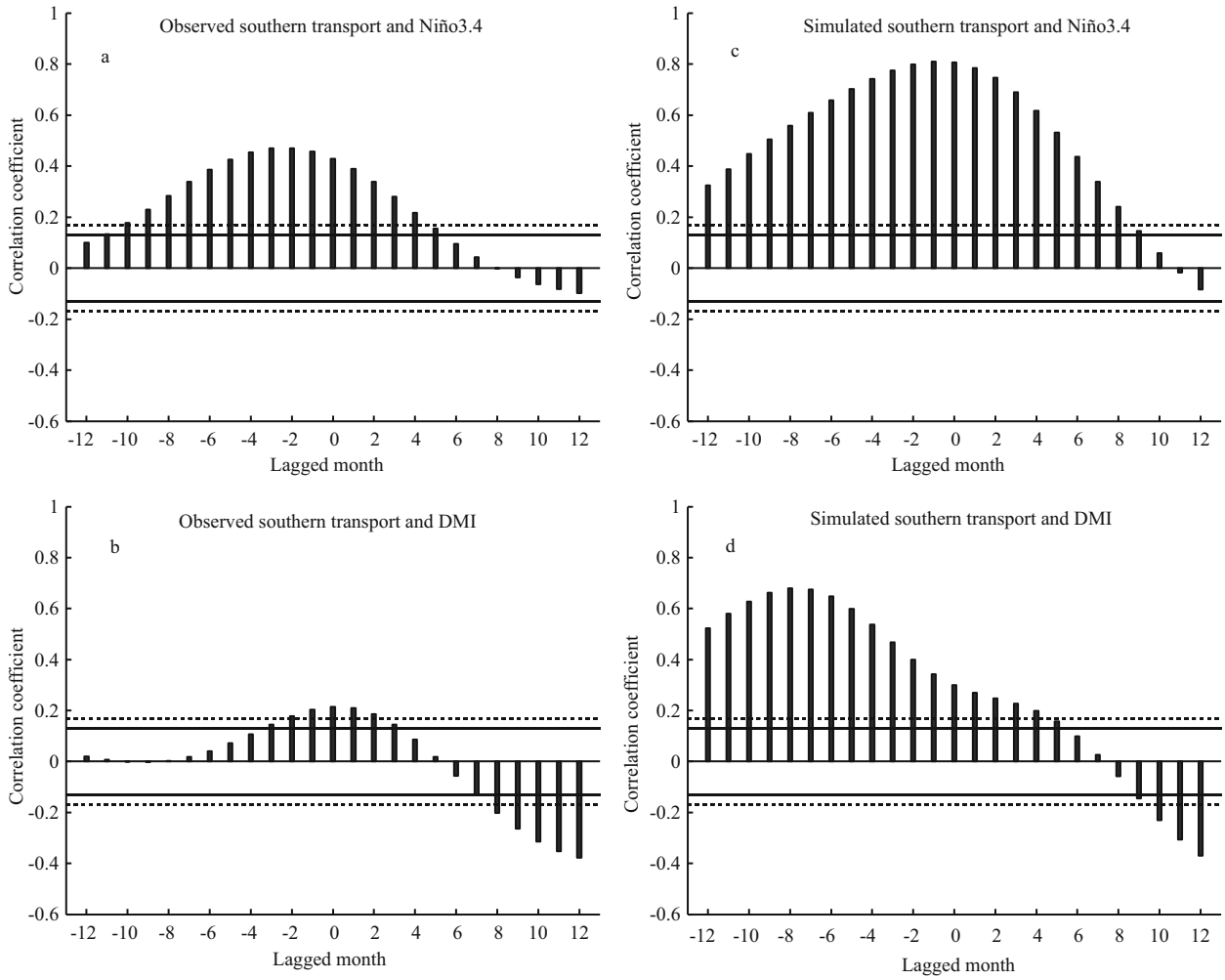

Fig.8 Comparison of observed (a, b) and simulated (c, d) lag correlations between the Niño3.4 and DMI indices and the southern geostrophic transport interannual anomalies from the northern Australian coast to 15°S across the IX1 section over the period of 1990 to 2008, respectively

Positive lagged months indicate that the southern anomalies lag the Niño3.4 or DMI index. Solid and dashed horizontal lines represent the 95% and 99% significance levels, respectively.

autumn and those in the cold tongue in the 1-year time lag than in the observations. This contradiction between the underestimated oceanic channel dynamics and the stronger lag correlations in the CGCM than in the observations is attributed to an overestimated atmospheric bridge process in the CGCM, which will be discussed in the following section.

3.6 Effects of the atmospheric bridge

Existing investigations of the atmospheric bridge process are based on correlation analyses between DMI and atmospheric anomalies. Yuan et al. (2013) pointed out that the use of DMI in the correlation analysis to evaluate the atmospheric bridge process is misleading, because the oceanic channel dynamics have been incorporated into the analysis through the use of the SSTA in the southeastern tropical Indian Ocean, which is closely associated with the upwelling anomalies off Java during the IOD. Instead, they suggested correlating the wind anomalies over the far western equatorial Pacific with the Pacific atmospheric anomalies to examine the variations of the Walker Circulation connecting the interannual variability over the two basins.

The lag correlations between the surface zonal wind anomalies (SZWA) averaged between 130°E and 150°E, 5°S and 5°N in autumn with the SZWA over the Indo-Pacific Oceans in the following winter through autumn in the CCSM4 simulation are compared with the observational analyses (Yuan et al., 2013) in Fig.10. The significant lag correlations in the simulated SZWA fields are clearly not supported by the observational analyses after the following

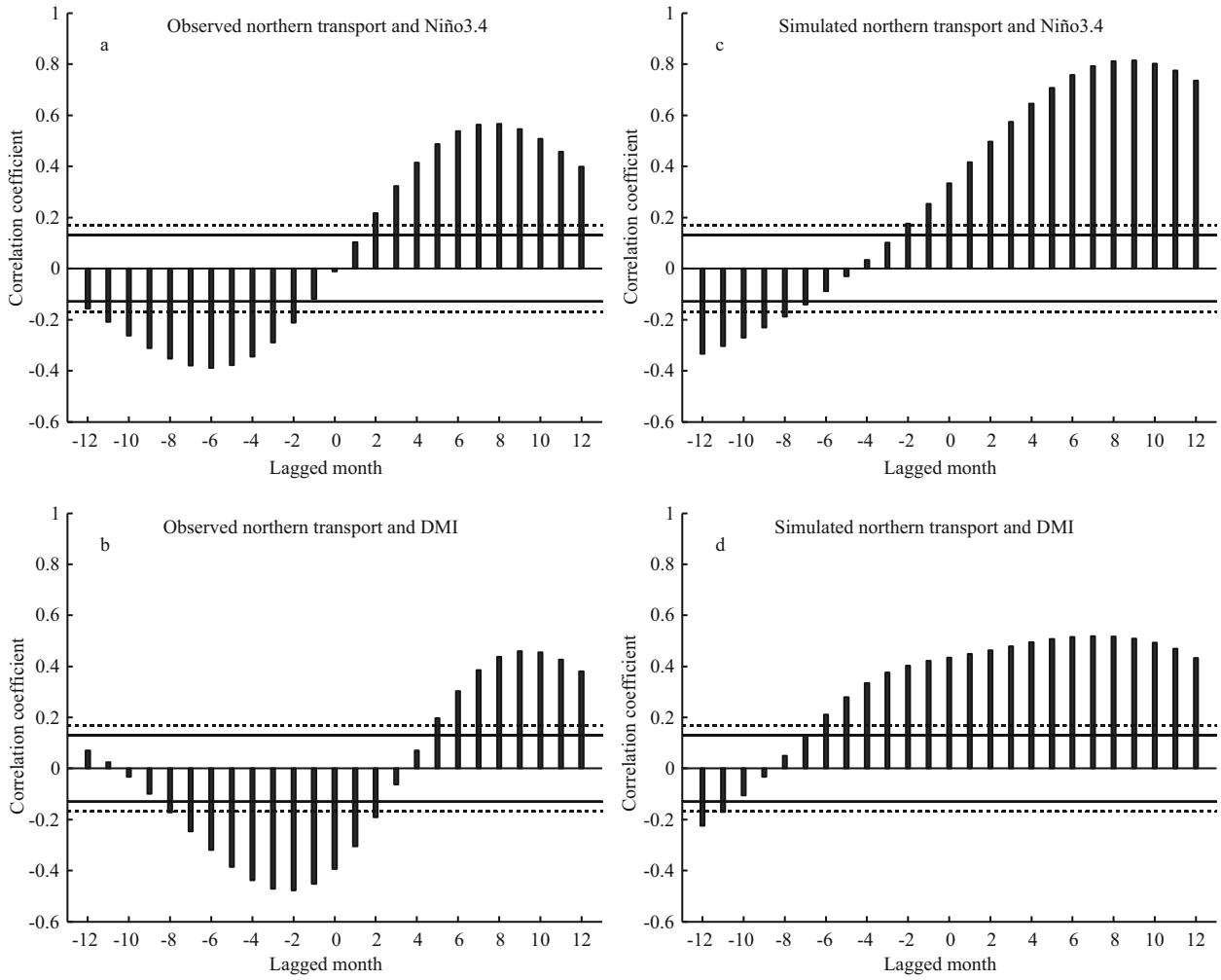

Fig.9 Comparison of observed (a, b) and simulated (c, d) lag correlations between the Niño3.4 and DMI indices and the northern geostrophic transport interannual anomalies from the southern Java coast to 15°S across the IX1 section over the period of 1990 to 2008, respectively

Positive lagged months indicate that the northern anomalies lag the Niño3.4 or DMI index. Solid and dashed horizontal lines represent the 95% and 99% significance levels, respectively.

winter. The unrealistic lag correlations in the western–central equatorial Pacific Ocean indicate unrealistic westerly wind anomalies over the equatorial Pacific in the CGCM simulation in Year 2 (Fig.10). These unrealistic wind anomalies generate upwelling equatorial Rossby waves propagating westward and downwelling equatorial Kelvin waves propagating eastward. The stronger subsurface lag correlations in the model than in the observations (Fig.5) can be explained by this wind patch. Similarly, the stronger lag correlations in the cold tongue in the 1-year time lag (Figs.3d, 4d) may be attributed to this wind patch. Thus, the weaker ITF anomalies in the CGCM simulation are overly compensated by the unrealistic wind patch when generating the subsurface anomalies in the equatorial vertical section of the Pacific Ocean.

The atmospheric bridge of the CGCM has been shown to produce significant negative lag correlations between the SZWA over the far western equatorial Pacific Ocean in autumn (Year 1) and in the eastern equatorial Pacific in the autumn of Year 2, and also creates significant positive correlations in the west, which are not supported by the observational analyses (Fig.10d). Evidently, the CGCM is unable to successfully simulate the observed atmospheric bridge process across the Indo-Pacific Oceans. In particular, the atmospheric bridge processes in the spring through autumn of Year 2 have been significantly overestimated.

As a result of the overestimated atmospheric bridge, the lag correlations between the SZWA over the far western equatorial Pacific in autumn and the SSHA in the cold tongue in the spring until autumn of Year 2 are all considerably stronger than in the

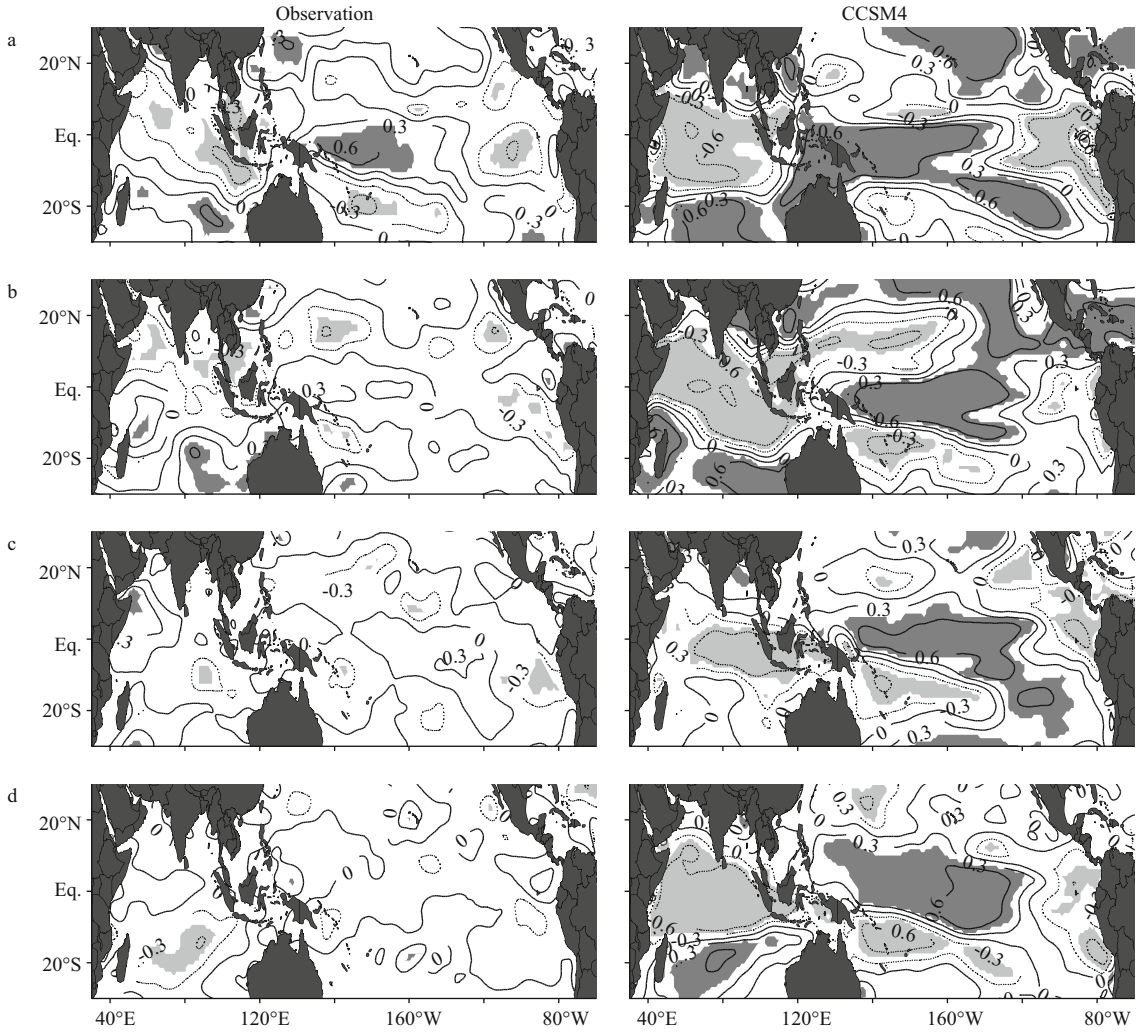

Fig.10 Comparison of observed (left column) and simulated (right column) lag correlations between the SZWA over the far western equatorial Pacific in autumn and the tropical Indo-Pacific SZWA in the following four seasons for the period of 1990 to 2009

a. winter (December to February); b. spring (March to May); c. summer (June to August); d. autumn (September to November). The contour interval is 0.3. Dark and light shades indicate positive and negative correlations significant at the 95% confidence level, respectively.

observations (Fig.11). This difference confirms that the model is unable to accurately simulate the atmospheric bridge processes observed in nature.

4 CONCLUSION

In this study, we assessed the skill of the CCSM4 climate system model in simulating the teleconnection between IOD in the Indian Ocean and ENSO in the Pacific Ocean in the 1-year time lag based on a comparison of analyses of the lag correlation with observational analyses. An experiment of the CCSM4 was chosen from the CMIP5 project data, based on a comparison of the simulated Niño3.4 time series with that observed during 1990–2009. A shift of the time coordinate of the CCSM4 experiment was implemented to fit a strong El Niño event of the simulation with the 1997–1998 El Niño. The model was shown to simulate the periodicity and recurrence of the ENSO events in the 1990s well. The spectrum analyses confirmed the good simulation of the El Niño events and IOD events by the CGCM. The spatial structure and phase-locking with the autumn season of the IOD year were also simulated successfully by the CCSM4 experiment.

In agreement with the observational analyses, the model has reproduced well the significant lag correlations between the SSTA in the southeastern tropical Indian Ocean in autumn and the cold tongue SSTA in the eastern equatorial Pacific 1 year later. The propagation of the SSHA from the southeastern tropical Indian Ocean to the Indonesian seas, inducing anomalous ITF transport and subsurface temperature

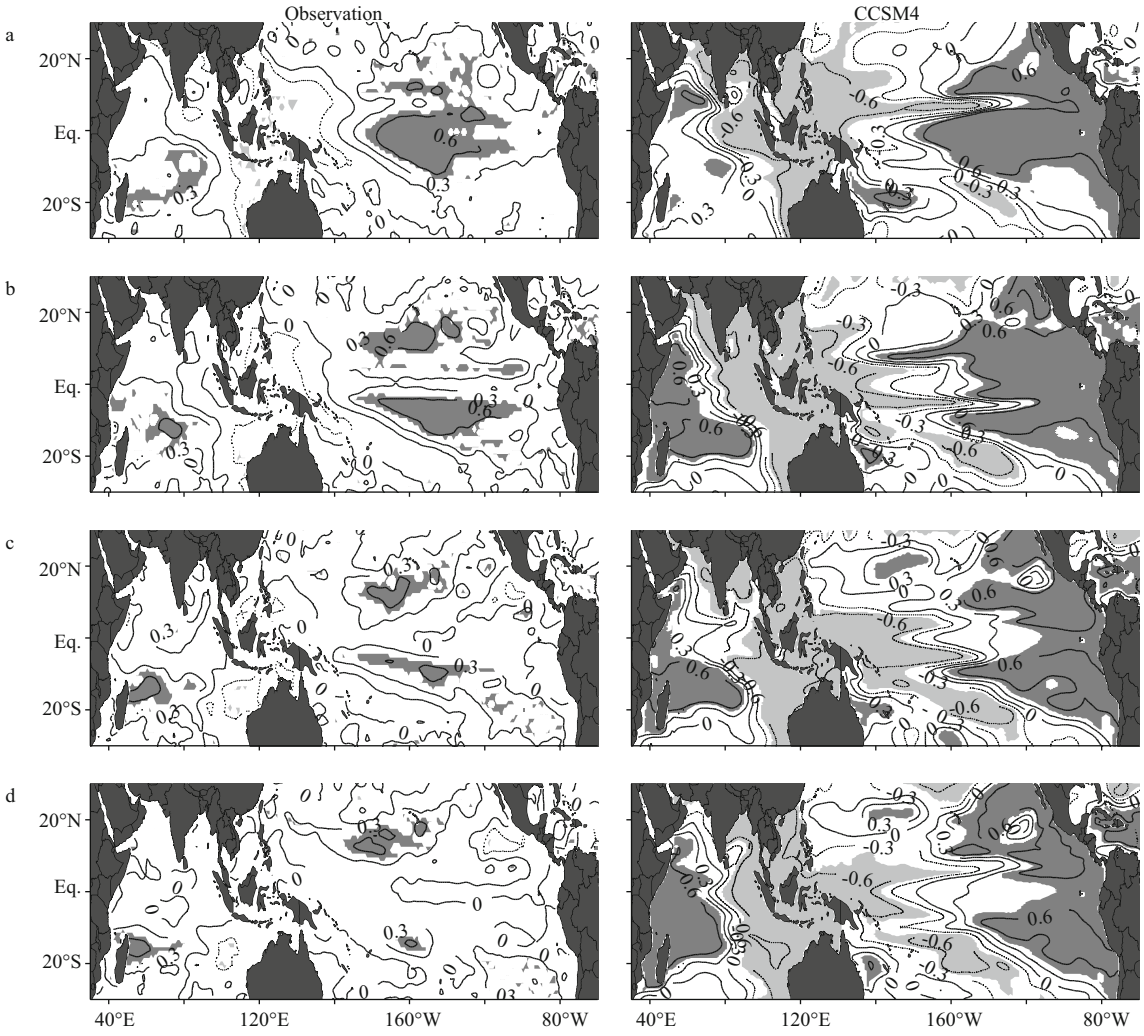

Fig.11 Comparison of observed (left column) and simulated (right column) lag correlations between the SZWA over the far western equatorial Pacific in autumn and the tropical Indo-Pacific SSHA in the following four seasons for the period of 1993 to 2009

a. winter (December to February); b. spring (March to May); c. summer (June to August); d. autumn (September to November). The contour interval is 0.3. Dark and light shades indicate positive and negative correlations significant at the 95% confidence level, respectively.

anomalies in the western equatorial Pacific Ocean (as evidenced by the propagation of positive lag correlations), is also simulated well by the CGCM. The significant lag correlations between the southeastern tropical Indian Ocean and the eastern Pacific oceanic anomalies and the propagation of the SSHA lag correlations across the Indo-Pacific basins were found to be independent of the tropical air-sea coupling, consistent with observational analyses. The lag correlations and the propagation of the SSHA suggest that the oceanic channel dynamics, namely the ITF variability, play an important role in connecting the IOD in the Indian Ocean with ENSO in the Pacific Ocean 1 year later.

However, the CCSM4 simulation has produced the stronger lag correlations between the southeastern tropical Indian Ocean and the eastern Pacific oceanic anomalies that were exhibited over a larger longitudinal domain in the central-eastern equatorial Pacific than the observations. In contrast, the oceanic channel dynamics were underestimated in the simulation according to the analyses of ITF geostrophic transport interannual anomalies across the IX1 section in the southeastern tropical Indian Ocean. The contradiction is attributed to the unrealistic westerly wind anomalies over the western-central equatorial Pacific in the year after IOD in the CCSM4 simulation. The unrealistic wind patch explains the higher lag correlations between the SSTA (SSHA) in the southeastern tropical Indian Ocean and the cold tongue SSTA (SSHA) in the 1-year time lag in the model than in the observations. The analyses therefore

suggest that the CCSM4 experiments overestimated the atmospheric bridge and underestimated the oceanic channel dynamics.

The importance of the oceanic channel dynamics for the predictability of ENSO over 1 year suggests that the connection between IOD and the ITF geostrophic transport in CCSM4 needs to be enhanced. A realistic simulation of the atmospheric bridge over the Indo-Pacific Oceans in the model is also necessary. The model has clearly produced an unrealistic atmospheric connection between the Indian and Pacific Oceans. This connection across the Indonesian seas must be reduced to improve the model skill in simulating and predicting ENSO.

Recent studies suggest the asymmetric transitivity between El Niño and La Niña (An et al., 2005; Ohba and Ueda, 2009a; Ohba et al., 2010; Okumura et al., 2011; Dommenget et al., 2013; Ohba, 2013). Future studies should investigate the forcing effects of the positive and negative IOD events on ENSO variability and predictability separately.

5 ACKNOWLEDGEMENT

We thank the WCRP CMIP project for sharing the model outputs.

References

Alexander M A, Bladé I, Newman M, Lanzante J R, Lau N C, Scot J D. 2002. The atmospheric bridge: the influence of Enso teleconnections on air-sea interaction over the global oceans. *J. Climate*, **15**(16): 2 205-2 231.

An S I, Ham Y G, Kug J S, Jin F F, Kang I S. 2005. El Niño La Niña asymmetry in the coupled model intercomparison project simulations. *J. Climate*, **18**(14): 2 617-2 627.

Annamalai H, Xie S P, McCreary J P, Murtugudde R. 2005. Impact of Indian Ocean sea surface temperature on developing El Nino. *J. Climate*, **18**(2): 302-319.

Clarke A J, Liu X. 1994. Interannual sea level in the northern and eastern Indian Ocean. *J. Phys. Oceanogr.*, **24**(6): 1 224-1 235.

Clarke A J, van Gorder S. 2003. Improving El Niño prediction using a space-time integration of Indo-Pacific winds and equatorial Pacific upper ocean heat content. *Geophys. Res. Lett.*, **30**(7), http://dx.doi.org/10.1029/2002GL016673.

Craig A P, Vertenstein M, Jacob R. 2012. A new flexible coupler for earth system modeling developed for CCSM4 and CESM1. *Int. J. High Perform. Comput. Appl.*, **26**(1): 31-42.

Dommenget D, Bayr T, Frauen C. 2013. Analysis of the non-linearity in the pattern and time evolution of El Niño southern oscillation. *Climate Dynamics*, **40**(11-12): 2 825-2 847.

Gent P R, Danabasoglu G, Donner L J, Holland M M, Hunke E C, Jayne S R, Lawrence D M, Neale R B, Rasch P J, Vertenstein M, Worley P H, Yang Z L, Zhang M H. 2011. The community climate system model version 4. *J. Climate*, **24**: 4 973-4 991.

Hunke E C, Lipscomb W H. 2008. CICE: the los alamos sea ice model, documentation and software user's manual, version 4.0. Los Alamos National Laboratory. Technology Report, LA-CC-06-012.

Izumo T, Vialard J, Lengaigne M, Montegut C D B, Behera S K, Luo JJ, Cravatte S, Masson S, Yamagata T. 2010. Influence of the state of the Indian Ocean Dipole on the following year's El Niño. *Nat. Geosci.*, **3**(3): 168-172.

Kalnay E, Kanamitsu M, Kistler R et al. 1996. The NCEP-NCAR 40-Year reanalysis project. *Bull. Am. Meteor. Soc.*, **77**(3): 437-472.

Klein S A, Soden B J, Lau N C. 1999. Remote sea surface temperature variations during ENSO: evidence for a tropical atmospheric bridge. *J. Climate*, **12**(4): 917-932.

Kug J S, Kang I S. 2006. Interactive feedback between ENSO and the Indian Ocean. *J. Climate.*, **19**(9): 1 784-1 801.

Kug J S, Li T, An S I, Kang I S, Luo J J, Masson S. 2006. Role of the ENSO-Indian Ocean coupling on ENSO variability in a coupled GCM. *Geophys. Res. Lett.*, **33**(9), http://dx.doi.org/10.1029/2005GL024916.

Lau N C, Leetmaa A, Nath M J, Wang H L. 2005. Influence of ENSO-induced Indo-Western Pacific SST anomalies on extratropical atmospheric variability during the boreal summer. *J. Climate*, **18**(15): 2 922-2 942.

Lau N C, Nath M J. 2003. Atmosphere-ocean variations in the Indo-Pacific sector during ENSO episodes. *J. Climate*, **16**(1): 3-20.

Lawrence D M, Oleson K W, Flanner M G, Thornton P E, Swenson S C, Lawrence P J, Zeng X B, Yang Z L, Levis S, Skaguchi K, Bonan G B, Slater A G. 2011. Parameterization improvements and functional and structural advances in version 4 of the Community Land Model. *J. Adv. Model Earth Syst.*, **3**(1), http://dx.doi.org/10.1029/2011MS000045.

Luo J J, Zhang R C, Behera S K, Masumoto Y, Jin F F, Lukas R, Yamagata T. 2010. Interaction between El Niño and extreme Indian Ocean dipole. *J. Climate*, **23**(3): 726-742, http://dx.doi.org/10.1175/2009JCLI3104.1.

Meehl G A, Boer G J, Covey C et al. 2000. The coupled model intercomparison project (CMIP). *Bull. Am. Meteor. Soc.*, **81**(2): 313-318.

Meyers G, Bailey R J, Woorby A P. 1995. Geostrophic transport of Indonesian Throughflow. *Deep Sea Research Part I: Oceanographic Research Papers*, **42**(7): 1 163-1 174.

Meyers G. 1996. Variation of indonesian throughflow and the El Niño-southern oscillation. *J. Geophys. Res*, **101**(C5): 12 255-12 263.

Neale R B, Richter J, Park S, Lauritzen P H, Vavrus S J, Rasch P J, Zhang M H. 2013. The mean climate of the Community Atmosphere Model (CAM4) in forced SST and fully coupled experiments. *J. Climate*, **26**(14): 5 150-5 168.

Ohba M, Nohara D, Ueda H. 2010. Simulation of asymmetric ENSO transition in WCRP CMIP3 multimodel

experiments. *J. Climate*, **23**(22): 6 051-6 067.

Ohba M, Ueda H. 2005. Basin-wide warming in the equatorial Indian Ocean associated with El Niño. *SOLA*, **1**: 89-92, http://dx.doi.org//10.2151/sola.2005-024.

Ohba M, Ueda H. 2007. An impact of SST anomalies in the Indian Ocean in acceleration of the El Niño to La Niña transition. *J. Meteor. Soc. Japan*, **85**(3): 335-348.

Ohba M, Ueda H. 2009a. Role of nonlinear atmospheric response to SST on the asymmetric transition process of ENSO. *J. Climate*, **22**(1): 177-192.

Ohba M, Ueda H. 2009b. Seasonally different response of the Indian Ocean to the remote forcing of El Niño: linking the dynamics and thermodynamics. *SOLA*, **5**: 176-179.

Ohba M, Watanabe M. 2012. Role of the Indo-Pacific interbasin coupling in predicting asymmetric ENSO transition and duration. *J. Climate*, **25**(9): 3 321-3 335.

Ohba M. 2013. Important factors for long-term change in ENSO transitivity. *Int. J. Climatol.*, **33**(6): 1 495-1 509.

Okumura Y M, Ohba M, Deser C, Ueda H. 2011. A proposed mechanism for the asymmetric duration of El Niño and La Niña. *J. Climate*, **24**(15): 3 822-3 829.

Rayner N A, Parker D E, Horton E B, Folland C K, Alexander L V, Rowell D P, Kent E C, Kaplan A. 2003. Global analyses of sea surface temperature, sea ice, and night marine air temperature since the late nineteenth century. *J. Geophys. Res.*, **108**(D14), http://dx.doi.org/10.1029/2002JD002670.

Saji N H, Goswami B N, Vinayachandran P N, Yamagata T. 1999. A dipole mode in the tropical Indian Ocean. *Nature*, **401**(6751): 360-363.

Smith R D, Jones P W, Briegleb B et al. 2010. The parallel ocean program (POP) reference manual: ocean component of the community climate system model (CCSM). Los Alamos National Laboratory, LAUR-10-01853.

Taylor K E, Stouffer R J, Meehl G A. 2012. An overview of CMIP5 and the experiment design. *Bull. Am. Meteor. Soc.*, **93**(4): 485-498, http://dx.doi.org/10.1175/BAMS-D-11-00094.1.

White W B. 1995. Design of a global observing system for gyre-scale upper ocean temperature variability. *Prog. Oceanogr.*, **36**(3): 169-217.

Wijffels S E, Meyers G, Godfrey J S. 2008. A 20-yr average of the Indonesian Throughflow: regional currents and the interbasin exchange. *J. Phys. Oceanogr.*, **38**(9): 1 965-1 978.

Wijffels S E, Meyers G. 2004. An intersection of oceanic waveguides: variability in the Indonesian Throughflow region. *J. Phys. Oceanogr.*, **34**(5): 1 232-1 253.

Xie S P, Hu K M, Hafner J et al. 2009. Indian Ocean capacitor effect on Indo-western Pacific climate during the summer following El Niño. *J. Climate*, **22**(3): 730-747.

Xu T F, Yuan D L, Yu Y Q, Zhao X. 2013. An assessment of Indo-Pacific oceanic channel dynamics in the FGOALS-g2 coupled climate system model. *Adv. Atmos. Sci.*, **30**(4): 997-1 016, http://dx.doi.org/10.1007/s00376-013-2131-2.

Yuan D L, Wang J, Xu T F, Xu P, Hui Z, Zhao X. 2011. Forcing of the indian ocean dipole on the interannual variations of the tropical pacific ocean: roles of the Indonesian Throughflow. *J. Climate*, **24**(14): 3 593-3 608.

Yuan D L, Zhou H, Zhao X. 2013. Interannual climate variability over the tropical Pacific Ocean induced by the Indian Ocean Dipole through the Indonesian Throughflow. *J. Climate*, **26**(9): 2 845-2 861.